

Emergent Task Differentiation on Network Filters*

Mehdi Saghafi[†], Harry Dankowicz[†], and Whitney Tabor[‡]

Abstract. This paper aims to analyze the emergence of task differentiation in a model complex system, characterized by an absence of hierarchical control, yet able to exhibit coordinated behavior and collective function. The analysis focuses on linear network filters, i.e., networks of coupled linear oscillators with a differentiated steady-state response to exogenous harmonic excitation. It demonstrates how an optimal allocation of excitation sensitivities across the network nodes in a condition of resonance may be constructed either using global information about the network topology and spectral properties or through the iterated dynamics of a nonlinear, nonsmooth learning paradigm that only relies on local information within the network. Explicit conditions on the topology and desired resonant mode shape are derived to guarantee local asymptotic stability of fixed points of the learning dynamics. The analysis demonstrates the possibly semistable nature of the fixed point with all zero excitation sensitivities, a condition of system collapse that can be reached from an open set of initial conditions but that is unstable under the learning dynamics. Theoretical and numerical results also show the existence of periodic responses, as well as of connecting dynamics between fixed points, resulting in recurrent metastable behavior and noise-induced transitions along cycles of such connections. Structural additions to a core network that conserve desired spectral properties are proposed as a defensive mechanism for fault tolerance and shielding of the core against targeted harm.

Key words. network dynamics, linear filter, division of labor, piecewise-smooth system

AMS subject classifications. 90B10, 90C35, 82C20, 37N40

DOI. 10.1137/16M1084432

1. Introduction. In a multiagent complex system, task differentiation (often referred to as division of labor) affords a mechanism for achieving an optimal collective behavior that is distinct from the behavior of the individual agents [7, 25, 29]. In the absence of hierarchical control, or any a priori differentiation between agents, such task differentiation must be an emergent property of the system dynamics, a result of indirect or direct interactions between agents [30]. When task differentiation is associated with a collective function that enhances the fitness of the system in the presence of environmental constraints, the system dynamics should be sensitive to changes in these constraints [6, 46]. Indeed, the exact distribution of tasks between agents must exhibit some degree of plasticity in order to maintain the desired function of the overall system as environmental conditions change [36].

In societies of honey bees and other social insects, task differentiation ensures that an intricate symphony of survival is played without the presence of a conductor [13, 15]. The queen

*Received by the editors July 12, 2016; accepted for publication (in revised form) March 23, 2017; published electronically September 6, 2017.

<http://www.siam.org/journals/siads/16-3/M108443.html>

Funding: This material is based upon work supported by the National Science Foundation under grant BCS-1246920.

[†]Department of Mechanical Science and Engineering, University of Illinois at Urbana-Champaign, Urbana, IL 61801 (mehdi.saghafi@gmail.com, danko@illinois.edu).

[‡]Department of Psychology, University of Connecticut, Storrs, CT 06269 (whitney.tabor@uconn.edu).

bee provides neither leadership nor central coordination [40]. Worker bees mature through a succession of in-hive roles, including the rearing of brood and general cleaning, ultimately ascending into a fellowship of foragers, who explore the environment surrounding the hive and gather nectar for its sustenance. Primed by age, the distribution of tasks in a colony may vary also with the availability of food, the number of nonforaging bees, the birth rate of brood, the survival rate of foragers, and other environmental conditions [11, 18, 45]. Since no one bee is either aware of all of these factors or able to impose an assignment of tasks onto the members of the colony, information about such secondary (for the process of maturation) inputs may be transmitted across the colony, e.g., through the widespread release of low-volatility pheromones or piggybacking on a network of social interactions [22].

Inspired by experimental evidence of social regulation of division of labor in insect societies [27], this paper aims to explore a paradigm for task differentiation in a model complex system, entirely through local interactions. Our development stands in some contrast to threshold-based models of emergent division of labor in insect societies available in the literature (e.g., [3, 21, 34]) and makes no pretense as to any implications for social insects. Instead, in an effort to explore a physically (and possibly biologically) important collective behavior, the theoretical discussion considers a class of complex systems that we call (*linear*) *network filters*, networks of coupled linear oscillators with a differentiated, open-loop, steady-state response to exogenous harmonic excitation (cf. [16, 20, 31, 32, 43], but see also [24] for related analysis of linear viscoelastic polymer networks). Here, the complex system is interpreted as an input-output system and filtering is understood to represent a frequency-dependent amplification or attenuation of an incoming exogenous signal, as seen in the system's response.

The filters considered here are *passive* [9] in that all the energy that is present in the system is supplied by the exogenous signal, rather than by endogenous processes, as would be the case for an *active* filter. The frequency-dependent amplification that interests us is the resonant response of lightly damped network filters to excitation near a system's natural frequencies. Such resonant behavior is characterized by a large amplitude response also in the case of small excitation amplitudes, rendering the system particularly sensitive to excitation at such a frequency. Localized excitation at resonance is also associated with long-range propagation of the incoming energy through the network.

As shown in our analysis, the response of a network filter at resonance is scaled by a linear combination of the sensitivity of individual nodes to excitation. Accordingly, we formalize a notion of task differentiation in terms of the vector of excitation sensitivities and seek to identify optimal assignments of the elements of this vector, as well as propose and analyze a dynamic learning paradigm whereby such optimal assignments may be arrived at indirectly through an iterated process. In particular, while optimal assignments may be identified using information about the global network topology, we aim for a learning paradigm in which updates to nodal excitation sensitivities depend only on properties of the corresponding network neighborhoods [39]. The analysis of such a model process enables rigorous prediction of the conditions that must hold, e.g., in order for the optimal assignment to be a (locally in state space) asymptotically stable fixed point.

Interestingly, because of the nonsmooth dependence of the proposed learning updates on the current vector of excitation sensitivities, we find that the fixed point for which the resonant excitation is perfectly rejected by the filter may attract an open set of initial conditions, even

as trajectories based at other initial conditions arbitrarily close to this fixed point deviate from it by an $\mathcal{O}(1)$ amount after a single iterate. Such a semistable fixed point is a striking feature of our piecewise smooth learning dynamics. In the presence of noise, this feature allows for a geometric decay toward a *dysfunctional* state during an intermediate stage of the learning dynamics, followed by convergence toward an asymptotically stable state only once the distance to the dysfunctional state is of the same order of magnitude as the noise. We show that such metastable behavior is also found between noise-induced transitions connecting coexisting semistable fixed points. While simple to formulate, our learning dynamics thus exhibit complicated transient and asymptotic dynamics that, in some cases, ultimately achieve the desired assignment of excitation sensitivities, and in others predictably fail to do so.

Beyond the question of task differentiation, we rely on our network filter model to examine mechanisms for building resilience into a complex system (cf. [1, 10], but see also [8, 17, 33]). Here, we consider ways in which nodes may be added to an existing core network while preserving a selected natural frequency as well as the restriction of the corresponding mode shape to the core nodes. Such additional nodes increase the cross-section of the network to targeted harm but reduce the relative cross-section of the core nodes. We analyze two such mechanisms for network growth: through the addition of redundant nodes and neutral nodes, respectively. In the former case, for example, we demonstrate how arbitrary networks of redundant nodes may be appended to individual nodes of the core network and suggest a way for these to enable localized detection and repair of the failure of a core node.

In contrast to much work on artificial neural networks, our models assume fixed connection weights. They nevertheless afford a form of learning in which each node adjusts its degree of participation in the dynamics, based only on locally available information, and successful learning is defined as achieving an optimal response when the network is excited at resonance. Our network models are inherently linear, finite-dimensional, and open-loop, so effects of nonlinearity, time-delay, or feedback control on properties of system synchronization and self-organization (e.g., [12, 23, 26, 28, 38]) are not considered here. Consequently, the dysfunctional state corresponding to perfect attenuation of a resonant exogenous signal as a result of vanishing excitation sensitivities is inherently distinct from the phenomenon of amplitude death found in coupled networks of nonlinear oscillators (e.g., [19, 42]).

We organize the discussion below as follows. In section 2, we consider a sequence of network designs, proceeding first from the analysis of an infinite one-dimensional lattice without a boundary, through that of a periodic one-dimensional lattice, to the case of ultimate interest: a general finite network. We allow the infinite and periodic lattice formalisms to inspire both the technique of analysis and the response characteristics of interest in the finite networks for which boundary effects may be significant. In section 3, we investigate the question of filter design in terms of the structural modifications alluded to in the previous paragraph, as well as the learning dynamics that form a core contribution of this work. A discussion in section 4, grounded in theoretical and numerical observations of the learning dynamics, looks toward a general phenomenology and its implications for other kinds of networks. Several directions for future research are considered in the concluding section 5.

2. Network filters. In this paper, we designate as (linear) *network filters* systems of coupled linear oscillators that transform excitatory exogenous signals into an output response

with a differentiated dependence on the excitation frequency. We consider both the transient response to localized excitation, as well as the steady-state response to harmonic excitation applied to network nodes according to their *excitation sensitivity*. We associate the characteristics of the system response with spectral properties of the network, specifically its distribution of natural frequencies and corresponding mode shapes. We find it useful to consider first two special cases of network filters, for which closed-form analysis yields useful insights that translate also to the nontrivial topologies that are of primary concern in this paper.

2.1. An infinite lattice. Let the nodes along an infinite, one-dimensional lattice represent identical single-degree-of-freedom linear mechanical oscillators of unit mass, damping ratio ζ , and natural frequency Ω (cf. [20]). Allow for additional linear coupling with unit stiffness (but no damping) between neighboring nodes up to a distance p . Specifically, if the displacement of the n th node at time t is denoted by $u_n(t)$, then the infinite system of differential equations

$$(1) \quad \ddot{u}_n(t) + 2\zeta\Omega\dot{u}_n(t) + \Omega^2u_n(t) + \sum_{r=1}^p (2u_n(t) - u_{n+r}(t) - u_{n-r}(t)) = f_n(t), \quad -\infty < n < \infty$$

describes the response of the lattice to the exogenous excitation $\{f_n(t)\}_{n=-\infty}^{\infty}$.

The Fourier transform pair

$$(2) \quad \hat{u}_\mu(t) = \sum_{n=-\infty}^{\infty} u_n(t)e^{-i\mu n} \Leftrightarrow u_n(t) = \frac{1}{2\pi} \int_{-\pi}^{\pi} \hat{u}_\mu(t)e^{i\mu n} d\mu$$

and similarly for $f_n(t)$ and $\hat{f}_\mu(t)$ imply that $\hat{u}_\mu(t) = \hat{u}_{\mu+2\pi}(t)$ and $\hat{f}_\mu(t) = \hat{f}_{\mu+2\pi}(t)$ for all μ . Substitution in (1) then yields

$$(3) \quad \ddot{\hat{u}}_\mu(t) + 2\zeta\Omega\dot{\hat{u}}_\mu(t) + \Omega_\mu^2\hat{u}_\mu(t) = \hat{f}_\mu(t),$$

in terms of the *dispersion relation* $\Omega_\mu = \sqrt{\Omega^2 + 2p - 2\sum_{r=1}^p \cos \mu r}$ for which, consequently, $\Omega_\mu = \Omega_{\mu+2\pi} = \Omega_{-\mu}$. It follows that

$$(4) \quad \hat{u}_\mu(t) = \left(2\zeta\Omega\hat{u}_\mu(0) + \dot{\hat{u}}_\mu(0)\right) \hat{h}_\mu(t) + \hat{u}_\mu(0)\dot{\hat{h}}_\mu(t) + \left(\hat{f}_\mu * \hat{h}_\mu\right)(t),$$

where

$$(5) \quad \hat{h}_\mu(t) = e^{-\zeta\Omega t} \frac{1}{\Omega_\zeta} \sin \Omega_\zeta t, \quad \Omega_\zeta = \sqrt{\Omega_\mu^2 - \zeta^2\Omega^2},$$

and the convolution

$$(6) \quad \left(\hat{f}_\mu * \hat{h}_\mu\right)(t) = \int_0^t \hat{f}_\mu(\tau)\hat{h}_\mu(t-\tau) d\tau.$$

In the special case of *harmonic excitation*, i.e., $f_n(t) = a_n \cos \omega t \Leftrightarrow \hat{f}_\mu(t) = \hat{a}_\mu \cos \omega t$ for constant a_n and \hat{a}_μ , the convolution integral evaluates to

$$(7) \quad \hat{a}_\mu \frac{(\Omega_\mu^2 - \omega^2) \left(\cos \omega t - \dot{\hat{h}}_\mu(t)\right) + 2\zeta\Omega\omega \left(\sin \omega t - \frac{\Omega_\mu^2}{\omega} \hat{h}_\mu(t)\right)}{(\Omega_\mu^2 - \omega^2)^2 + 4\zeta^2\Omega^2\omega^2}.$$

As $t \rightarrow \infty$, this converges to the *steady-state oscillatory response*

$$(8) \quad \hat{u}_{\mu,ss}(t) = \hat{a}_\mu \frac{(\Omega_\mu^2 - \omega^2) \cos \omega t + 2\zeta\Omega\omega \sin \omega t}{(\Omega_\mu^2 - \omega^2)^2 + 4\zeta^2\Omega^2\omega^2}$$

with amplitude $\hat{a}_\mu/\sqrt{(\Omega_\mu^2 - \omega^2)^2 + 4\zeta^2\Omega^2\omega^2}$. Notably, for $\zeta < \Omega_\mu/\sqrt{2}\Omega$, as a function of the *excitation frequency* ω , the steady-state amplitude exhibits *resonance* for $\omega = \omega_\mu^* = \sqrt{\Omega_\mu^2 - 2\zeta^2\Omega^2}$. For $\zeta \ll 1$, the amplitude at the resonance peak equals $\hat{a}_\mu(2\Omega\Omega_\mu\zeta)^{-1} + \mathcal{O}(\zeta)$ and the half-power bandwidth of the peak equals $2\Omega\zeta + \mathcal{O}(\zeta^2)$, corresponding to a quality factor of $\Omega_\mu/2\Omega\zeta + \mathcal{O}(\zeta^2)$. For ω to the left of the resonance peak, the steady-state amplitude decays to its DC value of \hat{a}_μ/Ω_μ^2 . Finally, for $\omega \gg \Omega_\mu$, the steady-state amplitude is $\ll \hat{a}_\mu$.

The spatial dependence of the steady-state response to harmonic excitation is now obtained from the integral

$$(9) \quad u_{n,ss}(t) = \frac{1}{2\pi} \int_{-\pi}^\pi \hat{a}_\mu \frac{(\Omega_\mu^2 - \omega^2) \cos \omega t + 2\zeta\Omega\omega \sin \omega t}{(\Omega_\mu^2 - \omega^2)^2 + 4\zeta^2\Omega^2\omega^2} e^{i\mu n} d\mu$$

or, provided that $\hat{a}_{-\mu} = \hat{a}_\mu$,

$$(10) \quad u_{n,ss}(t) = \frac{1}{\pi} \int_0^\pi \hat{a}_\mu \frac{(\Omega_\mu^2 - \omega^2) \cos \omega t + 2\zeta\Omega\omega \sin \omega t}{(\Omega_\mu^2 - \omega^2)^2 + 4\zeta^2\Omega^2\omega^2} \cos \mu n d\mu.$$

For $\zeta \ll 1$, $\mathcal{O}(\zeta^{-1})$ contributions to this integral are concentrated around values of $\mu \in [0, \pi]$, for which Ω_μ lies within $\mathcal{O}(\zeta^2)$ of ω . Provided that $\hat{a}_\mu = \mathcal{O}(1)$ for such values, it follows that the resultant spatial shape is spread across a wide range of nodes. A more concentrated spatial shape results (from destructive interference in the integral) for $\zeta = \mathcal{O}(1)$ when $\omega \approx \Omega_\mu$ for some μ or for all values of ζ when $\omega \gg \Omega_\mu$ for all μ .

We illustrate these observations by considering the special case of $a_n = \delta_{n0} \Leftrightarrow \hat{a}_\mu = 1$ for all μ . For reference, in the left panel of Figure 1, we graph Ω_μ^2 against μ for $p = 1, \dots, 5$. As shown in the right panel of Figure 1, a resonant response with a broad spatial shape is obtained only for ω within some finite range. We find it informative to consider, in addition to the steady-state response to harmonic excitation, the free response given initial conditions induced by a finite-time, spatially bounded pulse of harmonic excitation. For small values of ζ , we expect that significant propagation of energy away from the source will be suppressed for excitation frequencies outside of a pass-band, corresponding again to the range of values of Ω_μ for $\mu \in [0, \pi]$. In Figure 2, we contrast the displacement time histories for two different values of ω , induced by a harmonic excitation pulse with $a_n = \delta_{n0}$ and duration $10\pi/\omega$.

2.2. A periodic lattice. Consider next the imposition of spatial periodicity on the infinite lattice discussed in subsection 2.1 (cf. [37]). Specifically, suppose that $u_n(t) = u_{n+N}(t)$ and $f_n(t) = f_{n+N}(t)$ for all n . In this case, the Fourier transform pair

$$(11) \quad \hat{u}_m(t) = \sum_{n=1}^N u_n(t) e^{-2\pi imn/N} \Leftrightarrow u_n(t) = \frac{1}{N} \sum_{m=1}^N \hat{u}_m(t) e^{2\pi imn/N}$$

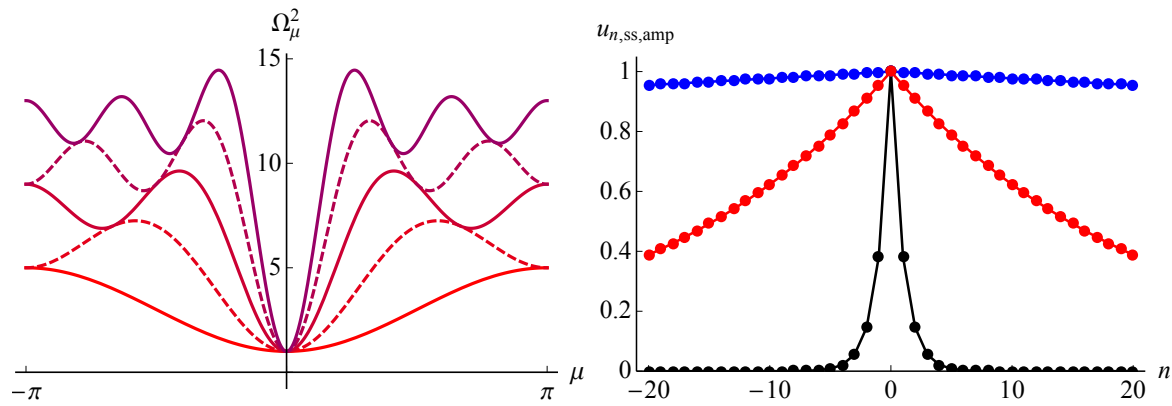


Figure 1. (Left panel) Graphical representation of the dispersion relation for the infinite lattice for $p = 1, \dots, 5$ with $\Omega = 1$. Here, $\Omega_\mu^2 \geq \Omega^2$ for all $\mu \in [-\pi, \pi]$ and $\Omega_\mu^2 = \Omega^2$ when $\mu = 0$, independently of p . Moreover, at $\mu = \pi$, $\Omega_\mu^2 = \Omega^2 + 2 + 2p$ for odd p and $\Omega_\mu^2 = \Omega^2 + 2p$ for even p . (Right panel) Steady-state response amplitudes $u_{n,ss,amp}$, in the case of $p = 1$, $\Omega = 1$, and $\zeta = 0.001$, to harmonic excitation at $n = 0$ with frequencies $\omega^2 = 4, 5$, and 6 (from top to bottom), normalized by the response at $n = 0$. A spatially bounded response is obtained for $\omega^2 = 6$, well outside of the pass-band defined by the dispersion relation.

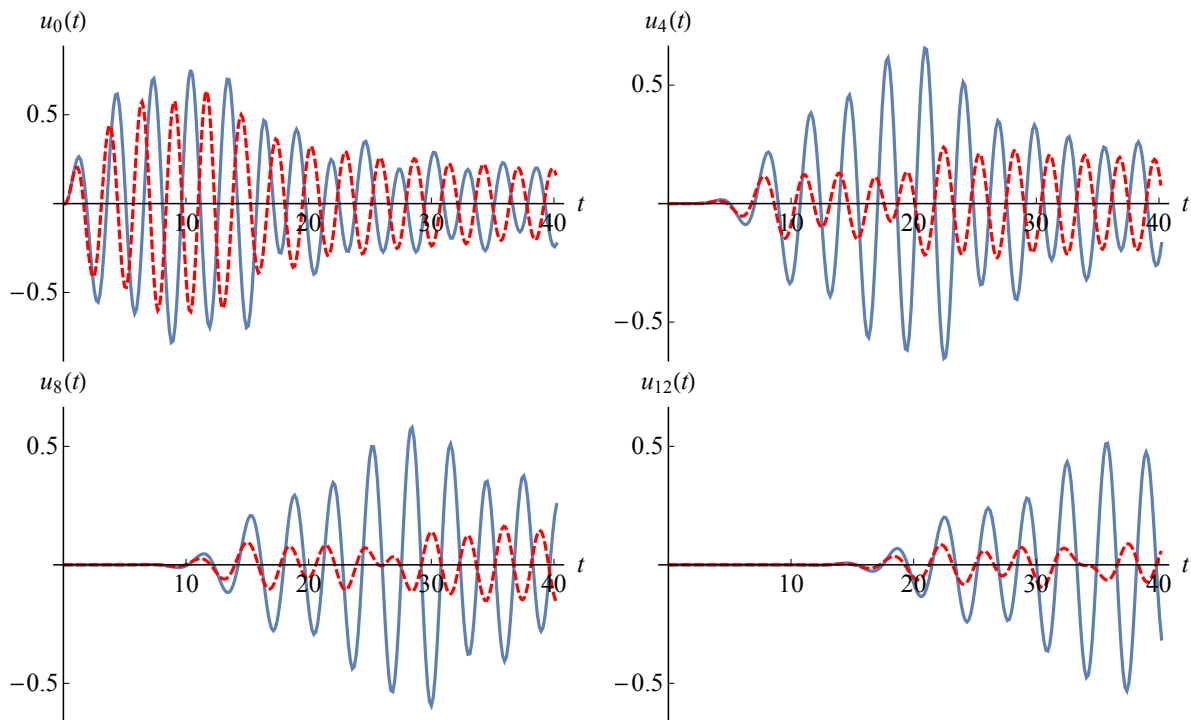


Figure 2. Transient response, for $p = 1$, from 5 periods of harmonic excitation at $n = 0$ at a frequency inside the pass-band ($\omega = 2$, solid) and outside the pass-band ($\omega = \sqrt{6}$, dashed). Here, $\zeta = 0.001$, $\Omega = 1$. The resonant case shows more significant propagation of energy to nodes far away from the point of excitation.

and similarly for $f_n(t)$ and $\hat{f}_m(t)$ imply that $\hat{u}_m(t) = \hat{u}_{m+N}(t)$ and $\hat{f}_m(t) = \hat{f}_{m+N}(t)$ for all m . Substitution in (1) and reference to the solution in (4) shows that

$$(12) \quad \hat{u}_m(t) = \left(2\zeta\Omega\hat{u}_m(0) + \dot{\hat{u}}_m(0)\right)\hat{h}_m(t) + \hat{u}_m(0)\dot{\hat{h}}_m(t) + \left(\hat{f}_m * \hat{h}_m\right)(t),$$

where

$$(13) \quad \hat{h}_m(t) = e^{-\zeta\Omega t} \frac{1}{\Omega_\zeta} \sin \Omega_\zeta t, \quad \Omega_\zeta = \sqrt{\Omega_m^2 - \zeta^2\Omega^2},$$

in terms of the dispersion relation $\Omega_m = \sqrt{\Omega^2 + 2p - 2\sum_{r=1}^p \cos \frac{2\pi mr}{N}}$ for $m \in \{1, \dots, N\}$.

Analogously to the treatment for the infinite lattice, in the limit of small damping, the amplitude of the oscillatory steady-state response to harmonic excitation behaves as $\mathcal{O}(\zeta^{-1})$ only for values of ω near a corresponding *natural frequency* Ω_m . The corresponding spatial dependence includes a linear combination of the spatially distributed *mode shapes* $\{\cos(2\pi mn/N)\}_{m=1}^N$ and $\{\sin(2\pi mn/N)\}_{m=1}^N$, as illustrated in the left panel of Figure 3. In contrast, for ω away from any natural frequency and sufficiently large N , we anticipate a spatially bounded steady-state response, as illustrated in the right panel Figure 3.

As with the infinite lattice, for small values of ζ , the free response induced by finite-time, spatially bounded pulses of harmonic excitation is expected to propagate more significantly across the network for frequencies near resonance. To illustrate this, Figure 4 shows the displacement time histories for two different values of ω , induced by a harmonic excitation

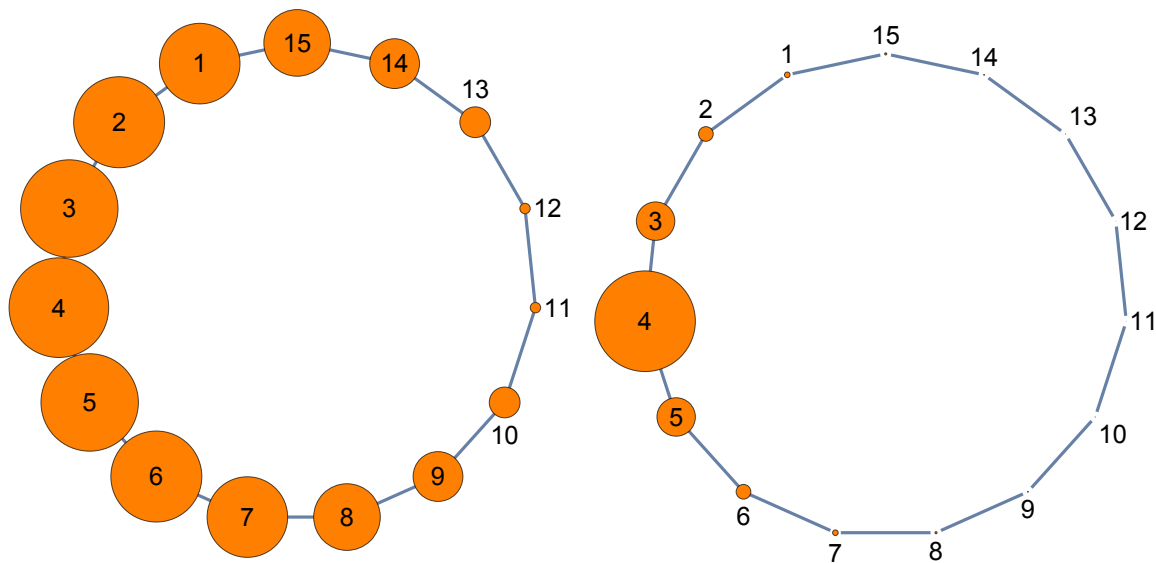


Figure 3. Spatially distributed steady-state shape at resonance (left panel) and spatially concentrated steady-state shape outside of the resonant band (right panel) for a periodic lattice with $N = 15$ and $p = 1$. Here, $\zeta = 0.001$, $\Omega = 1$, and $\omega \approx 2.23$ equals the largest natural frequency in the left panel and $\omega = \sqrt{6}$ in the right panel. In each case, excitation is introduced with unit magnitude at node 4 and the size of the nodes is scaled by the largest response amplitude. The actual amplitudes differ by two orders of magnitude between the panels.

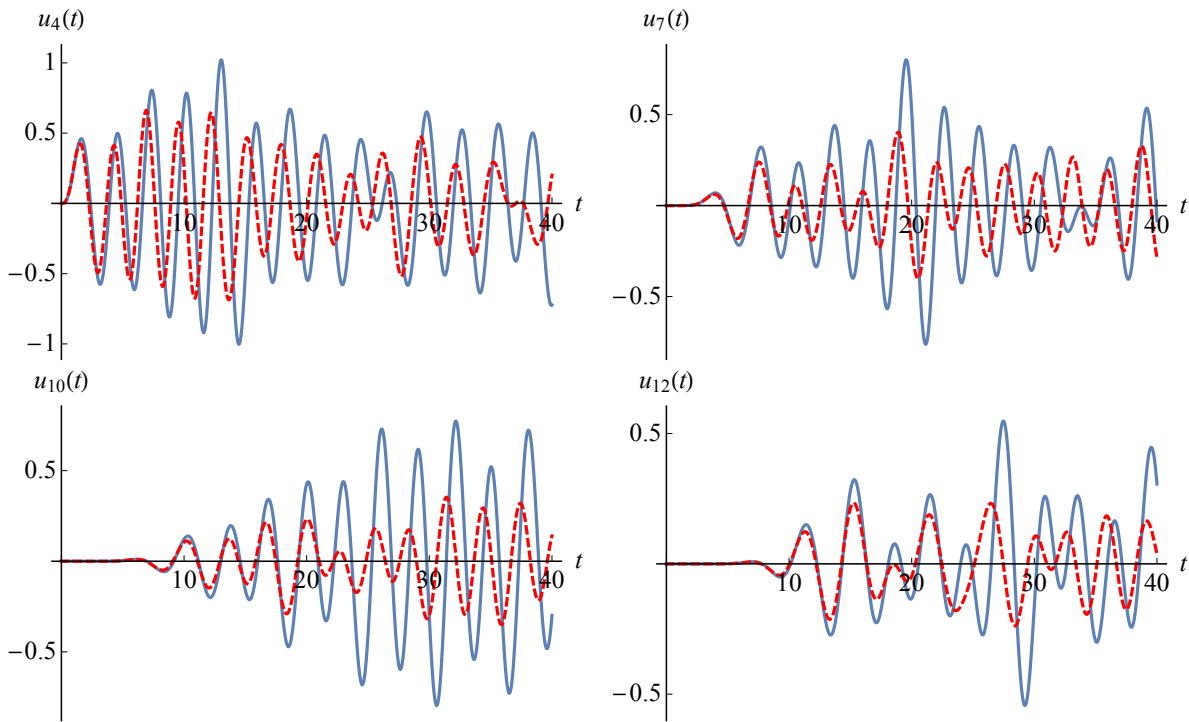


Figure 4. Transient response from 5 periods of harmonic excitation at node 4 in the network shown in Figure 3 at the largest resonance frequency ($\omega \approx 2.23$, solid) and with $\omega = \sqrt{6}$ (dashed). Here, $\zeta = 0.001$, $\Omega = 1$. The resonant case shows sustained larger amplitudes also at nodes far away from the point of excitation.

pulse with $a_n = \delta_{n4}$ and duration $10\pi/\omega$. In contrast to the infinite lattice, whose natural frequencies were given by a continuous spectrum Ω_μ for $\mu \in [-\pi, \pi]$, the periodic lattice is associated with a discrete spectrum Ω_m for $m \in \{1, \dots, N\}$. It follows from the dispersion relation that $\Omega_N = \Omega$ and $\Omega_m = \Omega_{N-m}$. For $m = N$, the corresponding mode shape is given by the sequence $\{1, \dots, 1\}$, while for $m \neq N$, $\sum_{n=1}^N e^{2\pi imn/N} = 0$, i.e., the sum of the positive components of a mode shape is equal in magnitude to the sum of its negative components.

2.3. General networks. We carry forward the observations from the infinite and periodic lattices to the case of an arbitrary finite uniform network of size N , wherein the neighborhoods of individual nodes are defined by a constant *adjacency matrix* A , such that $A_{i,j} = A_{j,i} = 1$ if nodes i and j are coupled, and 0 otherwise. It follows that the equation of motion for the vector $u(t)$ of displacements of the network nodes equals

$$(14) \quad \ddot{u}(t) + 2\zeta\Omega\dot{u}(t) + (L + \Omega^2 I) u(t) = f(t),$$

where the *network Laplacian* L is a symmetric, positive semidefinite matrix [4] for which $L_{i,j} = -A_{i,j}$ for $i \neq j$ and $L_{i,i} = \sum_j A_{i,j}$, and the components of the *excitation vector* $f(t)$ describe the exogenous force applied to the individual network nodes. We refer to the matrix sum $L + \Omega^2 I$ as the *global stiffness matrix*.

Let V denote a constant orthogonal matrix (cf. [44]) such that

$$(15) \quad V^T L V = \text{diag}\{\Omega_1^2 - \Omega^2, \dots, \Omega_N^2 - \Omega^2\}$$

for some sequence $\Omega \leq \Omega_N \leq \dots \leq \Omega_1$. By the definition of the Laplacian L , it follows that its smallest eigenvalue equals 0 (i.e., that $\Omega_N = \Omega$) and that the corresponding eigenspace includes the vector $(1 \cdots 1)^T$. Provided that this eigenspace is one-dimensional (i.e., that the network is connected), it follows by orthogonality that if v is an eigenvector corresponding to a nonzero eigenvalue, then

$$(16) \quad \sum_{i=1}^N v_i = 0,$$

i.e., the sum of all positive components of the eigenvector is equal in magnitude to the sum of all its negative components. In particular, this holds true for all but one of the columns of V .

The transform pairs $\hat{u}(t) = V^T u(t) \Leftrightarrow u(t) = V \hat{u}(t)$ and $\hat{f}(t) = V^T f(t) \Leftrightarrow f(t) = V \hat{f}(t)$ now imply that

$$(17) \quad \ddot{\hat{u}}_n(t) + 2\zeta\Omega\dot{\hat{u}}_n(t) + \Omega_n^2\hat{u}_n(t) = \hat{f}_n(t), \quad 1 \leq n \leq N.$$

The transient response to excitation and the steady-state response to harmonic excitation are again given by (4) and (8) with the substitution $\mu \mapsto n$. As with the periodic lattice (which corresponds to a diagonally banded, circulant adjacency matrix A [32]), in the limit of small damping, the steady-state amplitude behaves as $\mathcal{O}(\zeta^{-1})$ only for values of ω near a corresponding *natural frequency* Ω_m for some $m \in \{1, \dots, N\}$. If we assume a nondegenerate spectrum (i.e., $\Omega_m \neq \Omega_n$ for $m \neq n$), then the corresponding spatial dependence

$$(18) \quad u_{n,ss}(t) = \frac{V_{n,m}}{2\Omega\Omega_m\zeta} \sum_{k=1}^N V_{k,m} a_k \sin \omega t + \mathcal{O}(\zeta)$$

is dominated by the spatially distributed *mode shape* given by the m th column of V , scaled by the inner product between this column and the amplitude vector $a = (a_1 \cdots a_N)^T$. In contrast, for ω away from any resonance frequency and sufficiently large N , we anticipate a spatially concentrated steady-state response.

The left panels of Figure 5 show example resonant steady-state shapes for two connected networks with $N = 15$. The right panels show the spatially more concentrated response obtained for excitation frequencies away from resonance. Inspired by the observations for the infinite and periodic lattices, Figure 6 illustrates the propagation of energy through the network following single-node, finite-time pulses of harmonic excitation with frequencies near and away from resonance.

3. Network design. In the case of small damping, the networks discussed in section 2 are realizations of *frequency filters* that significantly amplify harmonic excitation signals with frequencies near a natural frequency, provided that the amplitude vector is aligned with the

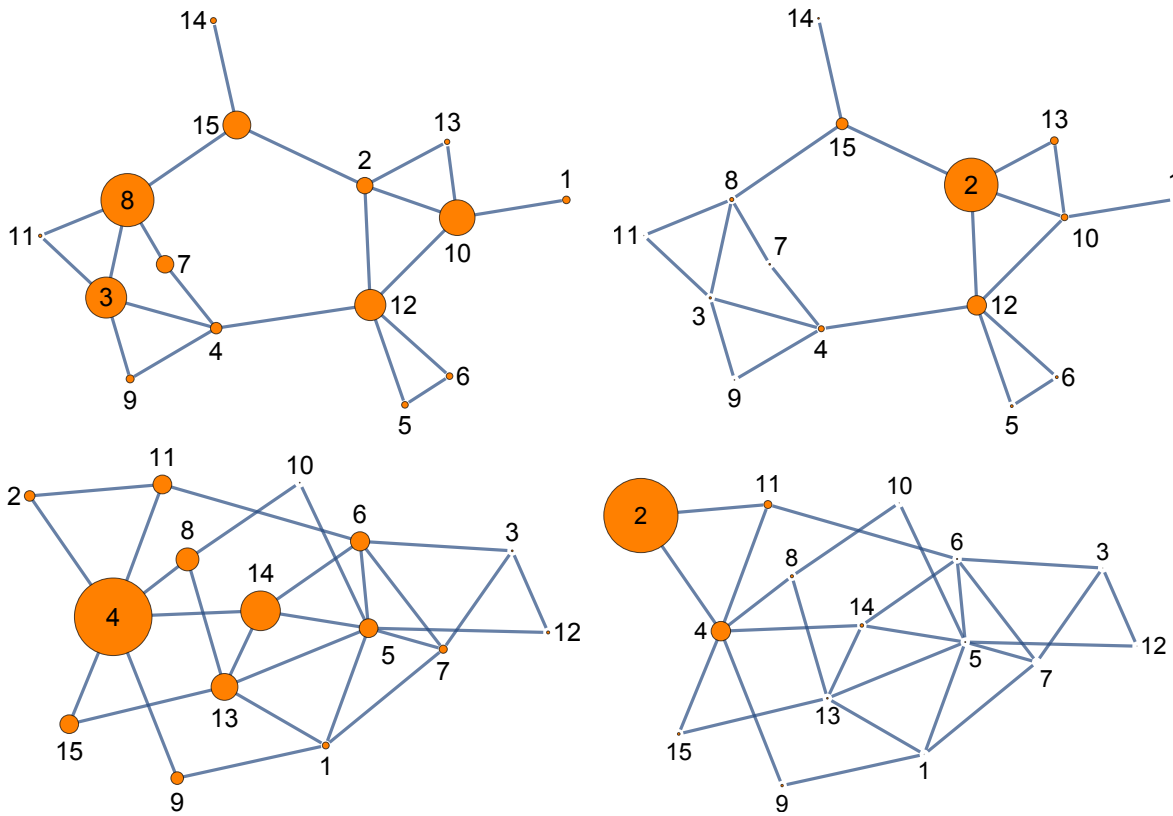


Figure 5. Spatially distributed steady-state shapes at resonance (left panels) and spatially concentrated steady-state shapes away from resonance (right panels). Here, $\zeta = 0.001$, $\Omega = 1$, and $\omega \approx 2.59$ (top) and $\omega \approx 2.93$ (bottom) equal the second largest natural frequencies in the left panels and $\omega = 3$ (top) and $\omega = \sqrt{11}$ (bottom), respectively, in the right panels. In each case, excitation is introduced with unit magnitude at node 2 and the size of the nodes is scaled by the largest response amplitude. The actual amplitudes differ by two orders of magnitude between the left and right panels.

corresponding mode shape. The relationship between the network structure and the resonance spectrum is encapsulated in the Laplacian matrix L and the subject of extensive previous research [4]. In the following, we make modest contributions to this theory by investigating the possibility of adding nodes to an existing network, while retaining a given natural frequency. We lay the foundation for an analysis of emergent *task differentiation* across the network by considering a dynamic game that seeks to optimize the alignment of an a priori undetermined amplitude vector and the corresponding mode shape, entirely through local interactions.

3.1. Network structure. We proceed to consider the addition of nodes to an existing finite network with discrete spectrum $\{\Omega_1, \dots, \Omega_N\}$. Specifically, we choose to require that such an addition preserve a selected resonance frequency and make predictable modifications to the corresponding mode shape. To this end, we allow for a differentiation between the grounding stiffness of nodes in the original network (for which this uniformly equals Ω^2) and the grounding stiffnesses of new nodes added to the network.

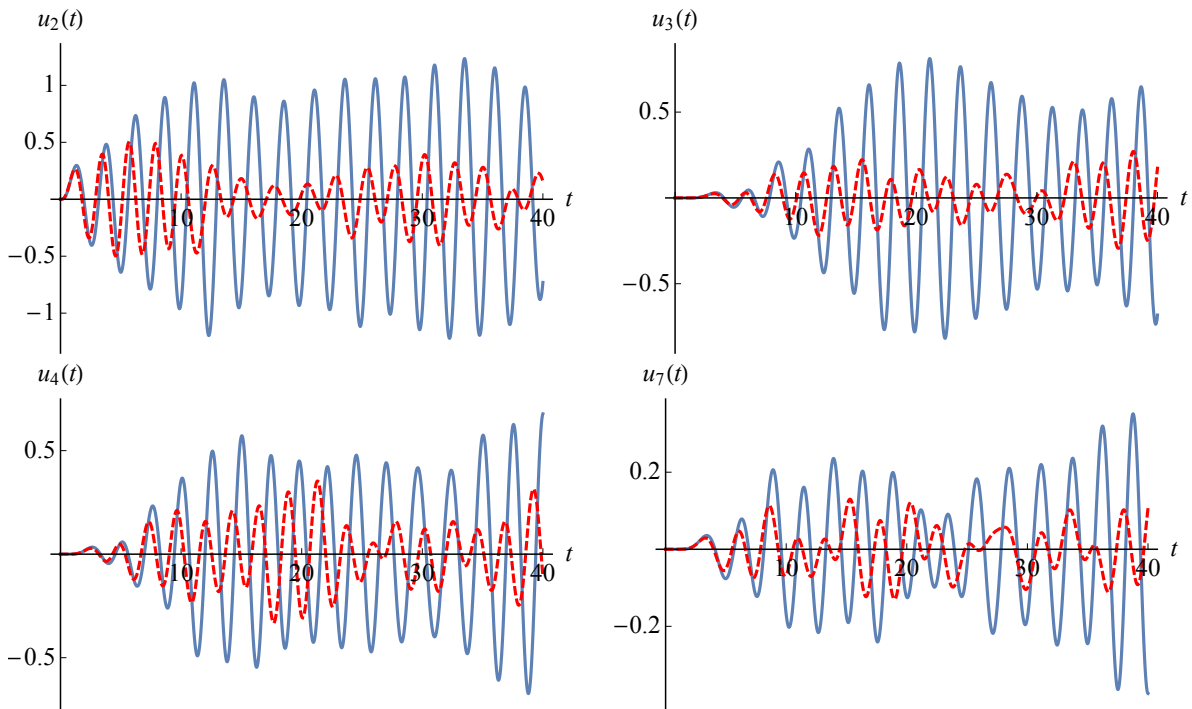


Figure 6. Transient response from 5 periods of harmonic excitation at node 2 in the network shown in the upper panels of Figure 5 at the second resonance frequency ($\omega \approx 2.59$, solid) and with $\omega = 3$ (dashed). Here, $\zeta = 0.001$, $\Omega = 1$. The resonant case shows significantly larger amplitudes also at nodes far away from the point of excitation.

Suppose, in particular, that a new node is connected to the k th node in the original network, and that the corresponding grounding stiffness is assigned to equal Ω_m^2 for some m , as shown in the left panel of Figure 7. The global stiffness matrix then takes the form

$$(19) \quad \begin{pmatrix} L + \text{diag}\{e_k\} + \Omega^2 & -e_k \\ -e_k^T & 1 + \Omega_m^2 \end{pmatrix},$$

where L denotes the original Laplacian and all components of the vector e_k equal 0 except for the k th which equals 1. If $Lv = (\Omega_m^2 - \Omega^2)v$, then

$$(20) \quad \begin{pmatrix} v \\ v_k \end{pmatrix}$$

is an eigenvector of (19) with eigenvalue Ω_m^2 . It follows that the spectrum of the expanded network retains the resonance frequency Ω_m .

Now suppose that a new node is connected to the l th node of the already expanded network and that the corresponding grounding stiffness again is assigned to equal Ω_m^2 , as shown in the left panel of Figure 7. The global stiffness matrix then takes the form

$$(21) \quad \left(\begin{pmatrix} L + \text{diag}\{e_k\} + \Omega^2 & -e_k \\ -e_k^T & 1 + \Omega_m^2 \end{pmatrix} + \text{diag}\{e_l\} \quad \begin{matrix} -e_l \\ \\ \\ 1 + \Omega_m^2 \end{matrix} \right).$$

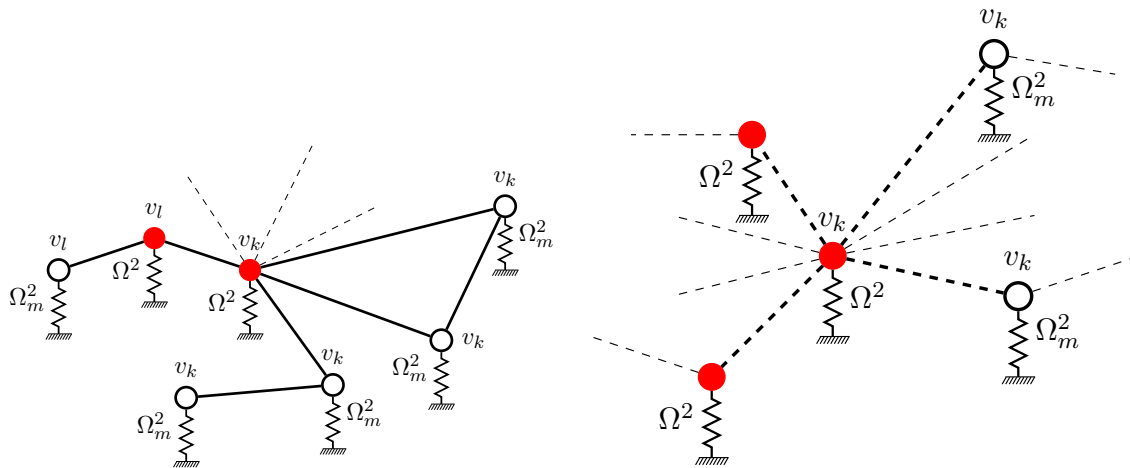


Figure 7. The addition of a single new node, pairs of new nodes, or rooted branches of new nodes (circles) to a core network (disks), as shown in the left panel, preserves a selected resonance frequency Ω_m and makes predictable modifications to the corresponding mode shape provided that the grounding stiffnesses of the new nodes equal Ω_m^2 . As suggested in the right panel, this observation generalizes to connecting a second network (circles) with arbitrary topology and uniform grounding stiffness Ω_m^2 to an arbitrary node in the original network (disks).

It follows by inspection that

$$(22) \quad \begin{pmatrix} v \\ v_k \\ v_l \end{pmatrix}$$

is an eigenvector of (21) with eigenvalue Ω_m^2 . By induction we may continue to grow the network while retaining resonance for $\omega = \Omega_m$, provided that all new nodes are connected to at most one node of the original network. In this case, all added nodes lie on rooted subtrees emanating from single nodes in the original network, and all nodes within the same subtree correspond to identical values for the corresponding components of the mode shape, as suggested in the left panel of Figure 7.

Suppose next that two new nodes in an already connected pair are connected to the k th and l th node, respectively, of the original network. Assume that the corresponding grounding stiffnesses are assigned the values

$$(23) \quad \frac{(\Omega_m^2 - 1)v_k + v_l}{v_k}$$

and

$$(24) \quad \frac{(\Omega_m^2 - 1)v_l + v_k}{v_l},$$

respectively, provided that these are both positive and finite. The global stiffness matrix then takes the form

$$(25) \quad \begin{pmatrix} L + \text{diag}\{e_k\} + \text{diag}\{e_l\} + \Omega^2 & -e_k & -e_l \\ -e_k^T & 2 + \frac{(\Omega_m^2 - 1)v_k + v_l}{v_k} & -1 \\ -e_l^T & -1 & 2 + \frac{(\Omega_m^2 - 1)v_l + v_k}{v_l} \end{pmatrix}.$$

It follows that

$$(26) \quad \begin{pmatrix} v \\ v_k \\ v_l \end{pmatrix}$$

is an eigenvector of (25) with eigenvalue Ω_m^2 .

In the special case that $k = l$, the above conclusions hold provided that the grounding stiffnesses for the two added nodes both equal Ω_m^2 , as also illustrated in the left panel of Figure 7. This observation implies that the nodes in the previously considered rooted subtrees may be connected arbitrarily within the tree without any changes to the resonance frequency or the corresponding mode shape. This is also immediately evident by the synchrony of their displacement time histories in resonance. It follows that an original network may be extended without affecting the resonance frequency Ω_m by connecting a second network with arbitrary topology and uniform grounding stiffness Ω_m^2 to an arbitrary node in the original network, as represented schematically in the right panel of Figure 7.

We conclude by investigating the addition of *neutral nodes*, i.e., nodes corresponding to a zero component of the mode shape associated with some resonance frequency. Specifically, consider a resonance frequency Ω_m of a network of nodes with identical grounding stiffnesses $\Omega^2 > 1$ and let v denote the corresponding mode shape. Suppose that a new node is connected to a subset Z of nodes in the original network, characterized by $\sum_{k \in Z} v_k = 0$, and that the grounding stiffnesses for these nodes are reduced by 1, as shown in the right panel of Figure 8.

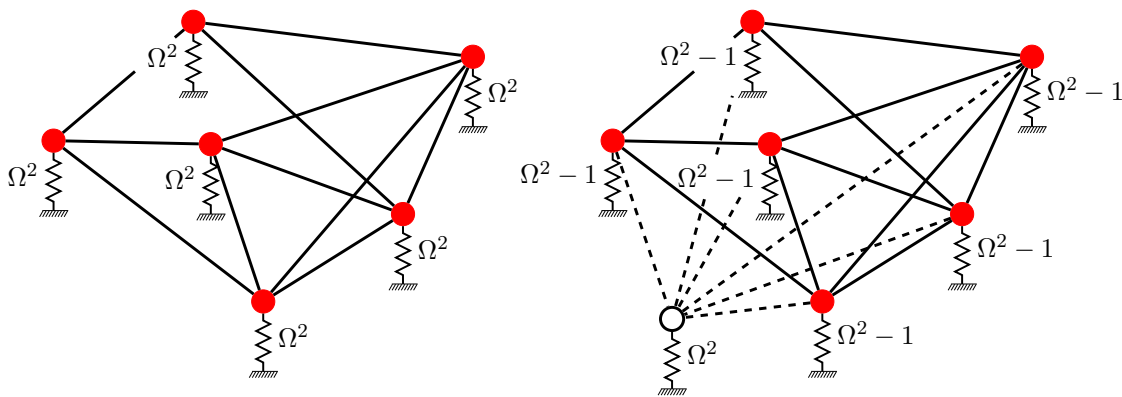


Figure 8. A neutral node (circle) may be added to a uniform core network (left panel) while preserving a given resonance frequency by attaching the new node to every node in the original network and reducing the old grounding stiffnesses by 1 (right panel). The same conclusion holds on a subset of nodes if the components of the corresponding mode shape cancel on this subset.

As observed previously, there exists at least one such subset, namely, $\{1, \dots, N\}$. The global stiffness matrix now takes the form

$$(27) \quad \begin{pmatrix} L + \Omega^2 & -e_Z \\ -e_Z^T & |Z| + \Omega^2 \end{pmatrix},$$

where all components of e_Z equal 0 except those indexed by elements of Z , which equal 1. It follows that

$$(28) \quad \begin{pmatrix} v \\ 0 \end{pmatrix}$$

is an eigenvector of (27) with eigenvalue Ω_m^2 . No change to the grounding stiffness of nodes with indices in Z is required if the corresponding component of v equals 0. If $Z = \{1, \dots, N\}$, then (28) is an eigenvector of the global stiffness matrix even without a change in grounding stiffness, albeit for the eigenvalue $\Omega_m^2 + 1$.

3.2. Response optimization. As suggested by (18), for $\zeta \ll 1$, the resonant response to harmonic excitation with frequency $\omega \approx \Omega_m$ scales by the dot product of the corresponding mode shape and the amplitude vector a . We choose to refer to each component of the amplitude vector as the *excitation sensitivity* of the corresponding node. If $a_k = 0$, then the steady-state response of the k th node is entirely due to coupling within the network, rather than direct excitation. We refer to such a node as a *receiving node*. A node with nonzero excitation sensitivity is a *sending node* that is directly excited and whose motion induces an oscillatory response among its neighbors. It is clear that the excitation sensitivity of neutral nodes has a negligible effect on the resonant steady-state response.

Restrict attention to the case where $a_k \in [0, 1]$ for $k \in \{1, \dots, N\}$ and $m > 1$. Since $\|u_{ss}(t)\| \sim |\sum_{k=1}^N V_{k,m} a_k|$, it follows from (16) that, for a network with identical grounding stiffnesses, $\|u_{ss}(t)\|$ may be maximized by either assigning $a_k = 1$ if $V_{k,m} > 0$ and $a_k = 0$ otherwise, or $a_k = 1$ if $V_{k,m} < 0$ and $a_k = 0$ otherwise. The addition of nodes with differentiated grounding stiffnesses, as in subsection 3.1, breaks the symmetry encoded in (16). In this case, an optimal alignment that maximizes $\|u_{ss}(t)\|$ is given by one of the two choices considered in the presence of symmetry.

The assignment of optimal excitation sensitivities for a given resonance frequency imposes a form of task differentiation across the network by designating a subset S of sending nodes with $a_k = 1$ for $k \in S$ and designating its complement $\{1, \dots, N\} \setminus S$ as the set of receiving nodes. As an example, Figure 9 shows resonant steady-state shapes and optimal selections of the subset S for two uniform networks and example mode shapes.

As discussed in subsection 3.1, the overall steady-state response of a network to harmonic excitation at Ω_m may be augmented by appending a second arbitrary network with uniform grounding stiffness Ω_m^2 to an arbitrary sending node in the original network and designating all new nodes as sending nodes. Moreover, the optimal differentiation is unchanged by the addition of neutral nodes per the recipe discussed in subsection 3.1.

Although the optimal assignment of nodes to S and its complement is straightforward at the global network level, we are interested in exploring a *learning algorithm*, whereby values in $[0, 1]$ for the excitation sensitivities are arrived at dynamically, based only on local interactions

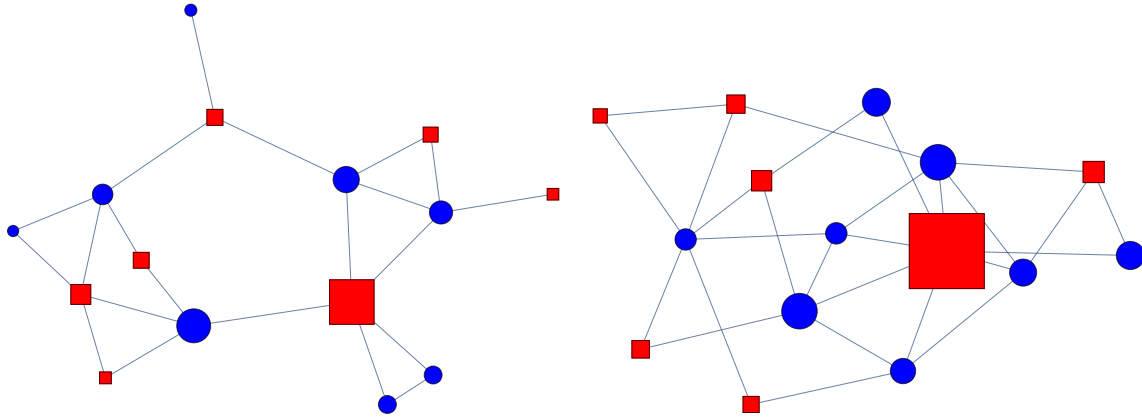


Figure 9. Graphical representation of the mode shape corresponding to the largest natural frequency for each of two uniform connected networks with 15 nodes and 21 ($\Omega_1^2 - \Omega^2 \approx 6.64$) and 27 edges ($\Omega_1^2 - \Omega^2 \approx 8.30$), respectively. Here, circles (blue) and squares (red) denote positive and negative elements of the corresponding eigenvector. The size of each vertex is affine in the magnitude of the corresponding element. Optimal selections for the subset S discussed in the text are obtained either from the subset of blue circles or of red squares.

within the network. Specifically, we seek a discrete-time model for network learning of an optimal design of a that maximizes the function $a \mapsto |v^T a|$ for some vector v , assumed below to equal an eigenvector of L . In particular, we explore a model wherein learning updates applied to a_n depend only on the components of a and v for the n th node and its immediate neighbors. When such a local learning approach is able to achieve globally optimal choices, we speak of *emergent coordination* or *emergent task differentiation*. We are interested not only in conditions that ensure such emergent coordination but also in conditions for which circumstances conspire against global coordination.

Let P_+ , P_0 , and P_- denote the subsets of $\{1, \dots, N\}$ corresponding to positive, zero, and negative components of v , respectively. Suppose, without loss of generality, that $\sum_{k \in P_+} v_k \geq -\sum_{k \in P_-} v_k$. The quantity $|v^T a|$ is then maximized by $a_k = 1$ for $k \in P_+$ and 0 otherwise. We proceed to define *simultaneous* updates to the components of a corresponding to one iterate of network learning. Specifically, for $n \in P_0$, suppose that $a_n \mapsto 0$. For $n \notin P_0$, let \mathcal{F}_n be a subset of $\{1, \dots, N\}$ representing the corresponding network neighborhood (excluding the n th node). Then, with $g_n = \sum_{k \in \mathcal{F}_n} v_k a_k$ and given a learning rate $\rho \in [0, 1]$, let

$$(29) \quad a_n \mapsto \begin{cases} \rho + (1 - \rho)a_n & \text{if } g_n v_n > 0, \\ (1 - \rho)a_n & \text{if } g_n v_n < 0, \\ a_n & \text{if } g_n = 0. \end{cases}$$

Apart from the trivial reset $a_n \mapsto 0$ for $n \in P_0$, the model exhibits no learning when $\rho = 0$. In the case that $\rho = 1$, $a \in \{0, 1\}^N$ after the first stage of learning (provided that $g_n \neq 0$), and jumps between 0 and 1 are instantaneous, rather than gradual as is the case when $0 < \rho < 1$.

3.3. Learning dynamics. A preliminary study of the possible learning dynamics is afforded by an analysis of its fixed points and their stability. Without loss of generality, remove nodes with indices in P_0 and assume that the remaining nodes form a connected network. When this does not hold, each connected component is a special case of the analysis below.

For any network topology, three trivial fixed points are given by (i) the zero vector $a^* = 0$, (ii) the optimal solution with $a_n = 1$ for $n \in P_+$ and 0 otherwise, since the latter implies that $g_n \geq 0$ for all n , and (iii) the potentially suboptimal solution with $a_n = 1$ for $n \in P_-$ and 0 otherwise, since the latter implies that $g_n \leq 0$ for all n . The existence of additional nontrivial fixed points depends both on the network topology and the vector v . For example, for every union U of connected components of P_+ (or of P_-), a fixed point is obtained by the assignment $a_n = 1$ for $n \in U$ and 0 otherwise.

Any fixed point with $g_n \neq 0$ for all n must be an element of $\{0, 1\}^N$, although the converse does not hold. By construction, such a fixed point is always locally asymptotically stable. Instability must therefore be associated with fixed points for which $g_k = 0$ for some k . For example, if $a_k \notin \{0, 1\}$ and $g_k = 0$ for some k , then any nonzero perturbation to g_k will result in a finite change to a_k , independent of the perturbation to g_k . Moreover, if $k \in P_+$ ($k \in P_-$), $a_k = 0$, $g_k = 0$, and $P_+ \cap \mathcal{F}_k \neq \emptyset$ ($P_- \cap \mathcal{F}_k \neq \emptyset$), then any positive (negative) perturbation to g_k will result in the assignment $a_k \mapsto \rho$. Similarly, if $k \in P_+$ ($k \in P_-$), $a_k = 1$, $g_k = 0$, and $P_- \cap \mathcal{F}_k \neq \emptyset$ ($P_+ \cap \mathcal{F}_k \neq \emptyset$), then any negative (positive) perturbation to g_k will result in the assignment $a_k \mapsto 1 - \rho$. In each case, the corresponding fixed point is unstable.

Provided that P_- is nonempty, the trivial fixed point at $a^* = 0$ is always unstable, since a perturbation with $a_k > 0$ for some k with $v_k > 0$ and $v_j < 0$ for some $j \in \mathcal{F}_k$ results in the assignment $a_j \mapsto \rho$. Nevertheless, it is straightforward to design examples for which $a = 0$ attracts an open set of initial conditions. Indeed, if the initial value of a ensures that $g_n v_n < 0$ for all n with $a_n \neq 0$, then this will remain true throughout learning and a will converge to $a^* = 0$ at the rate $1 - \rho$. Such an unstable fixed with an open inset is said to be *semistable*.

Consider, instead, the fixed point with $a_n = 1$ for $n \in P_+$ and 0 otherwise. If $g_k = 0$ for some k , then this fixed point is unstable, since $P_- \cap \mathcal{F}_k \neq \emptyset$. Similarly, if $g_k = 0$ for some k for the fixed point given by $a_n = 1$ for $n \in P_-$ and 0 otherwise, then this fixed point is unstable, since $P_+ \cap \mathcal{F}_k \neq \emptyset$. It follows that asymptotic stability is obtained provided that $P_+ \cap \mathcal{F}_n \neq \emptyset$ for every n in the former case, and $P_- \cap \mathcal{F}_n \neq \emptyset$ for every n in the latter case.

Now suppose that S is the largest subset of P_+ such that $S \cap \mathcal{F}_n \neq \emptyset$ for every $n \in S \cup P_-$. Then, provided that S is nonempty, the assignment $a_n = 1$ for $n \in S$ and 0 otherwise is an asymptotically stable fixed point. A similar conclusion again holds by substituting P_- for P_+ and vice versa. Any fixed point obtained by the assignment of $a_n = 1$ for n on some proper subset of such a set S and 0 otherwise must be unstable.

If the set of sending nodes for some fixed point includes nodes in both P_+ and P_- , then the fixed point is clearly suboptimal. Outside of the general conclusion regarding its stability in the case that $g_n \neq 0$ for all n , a case-by-case analysis must be applied.

Even with the existence of asymptotically stable fixed points, the learning dynamics may exhibit more complicated recurrence, e.g., period-2 orbits, in which two distinct values of the amplitude vector are visited in succession. The existence of such dynamics and their stability depend not only on the network topology and the vector v , but also on the learning rate ρ .

Finally, we expand on the observation made for the stability of the trivial fixed point at $a^* = 0$ and note that instability may be accompanied by semistable dynamics with insets with nonempty interiors. In this case, connecting dynamics between fixed points may be associated with one semistable fixed point being a limit point of the inset of a second fixed point and, quite possibly, vice versa. In the presence of noise, such connecting dynamics could result in persistent noise-induced cyclic transitions among a collection of fixed points or a finite sequence of distinct metastable dynamics followed by a final transition to an asymptotically stable recurrent behavior.

3.4. Numerical results. We explore the observations from subsection 3.3 in the context of a uniform network with $N = 15$ whose graph is shown in Figure 10. Here, each panel is differentiated by a mode shape v corresponding to some natural frequency of the global stiffness matrix. In all cases, $P_0 = \emptyset$ and $\sum_{k \in P_+} v_k = -\sum_{k \in P_-} v_k$.

In the top-left panel (largest natural frequency), the set $S = \{1, 2, 5, 9, 12, 13, 15\}$ is the largest subset of P_- such that $S \cap \mathcal{F}_n \neq \emptyset$ for every $n \in S \cup P_+$. By the theoretical analysis above, the assignment $a_n = 1$ for $n \in S$ and 0 otherwise (for which $v^T a \approx -0.83$) should result in an asymptotically stable fixed point. In contrast, there is no nonempty subset S of P_+ such that $S \cap \mathcal{F}_n \neq \emptyset$ for every $n \in S \cup P_-$. The two fixed points obtained by assigning $a_n = 1$ for $n \in \{6, 11\}$ ($v^T a \approx 0.052$) or $n \in \{8, 10, 14\}$ ($v^T a \approx 0.064$), respectively, and 0 otherwise are both semistable with open insets, as are the fixed point obtained by the combination of these assignments (for which $v^T a \approx 0.115$) and the trivial fixed point at $a^* = 0$. These claims are verified by the numerical simulations shown in Figure 11, where all dynamics are attracted by the asymptotically stable fixed point in the presence of noise, albeit allowing for metastable dynamics on approach to one of the other fixed points prior to convergence.

A distinct behavior is obtained for the mode shape (fourth largest natural frequency) represented by the bottom-right panel. Of the two fixed points obtained by assigning $a_n = 1$ for $n \in \{2, 6, 9, 12\}$ ($v^T a \approx -0.57$) or $n \in \{3, 5, 7, 13, 15\}$ ($v^T a \approx 1.00$) and 0 otherwise, we anticipate that the first is unstable (but with an open inset) and the second is asymptotically stable. These claims are verified by the numerical simulations shown in Figure 12, which include recurrent, noise-induced connecting transitions between the former fixed point and that obtained by also letting $a_7 = 1$ (for which $v^T a \approx -0.565$). Interestingly, for $\rho = 0.8$, simulations also reveal two period-2 attractors, in one case switching between

$$(30) \quad a = (0 \quad 1/6 \quad 1 \quad 0 \quad 5/6 \quad 5/6 \quad 1 \quad 0 \quad 0 \quad 0 \quad 0 \quad 0 \quad 1 \quad 0 \quad 1)^T$$

with $v^T a \approx 0.62$ and

$$(31) \quad a = (0 \quad 5/6 \quad 1 \quad 0 \quad 1/6 \quad 1/6 \quad 1 \quad 0 \quad 0 \quad 0 \quad 0 \quad 0 \quad 1 \quad 0 \quad 1)^T$$

with $v^T a \approx 0.14$ and in the other between

$$(32) \quad a = (0 \quad 1 \quad 1/6 \quad 0 \quad 5/6 \quad 5/6 \quad 1 \quad 0 \quad 1 \quad 0 \quad 0 \quad 1 \quad 0 \quad 0 \quad 1/6)^T$$

with $v^T a \approx 0.17$ and

$$(33) \quad a = (0 \quad 1 \quad 5/6 \quad 0 \quad 1/6 \quad 1/6 \quad 1 \quad 0 \quad 1 \quad 0 \quad 0 \quad 1 \quad 0 \quad 0 \quad 5./6)^T$$

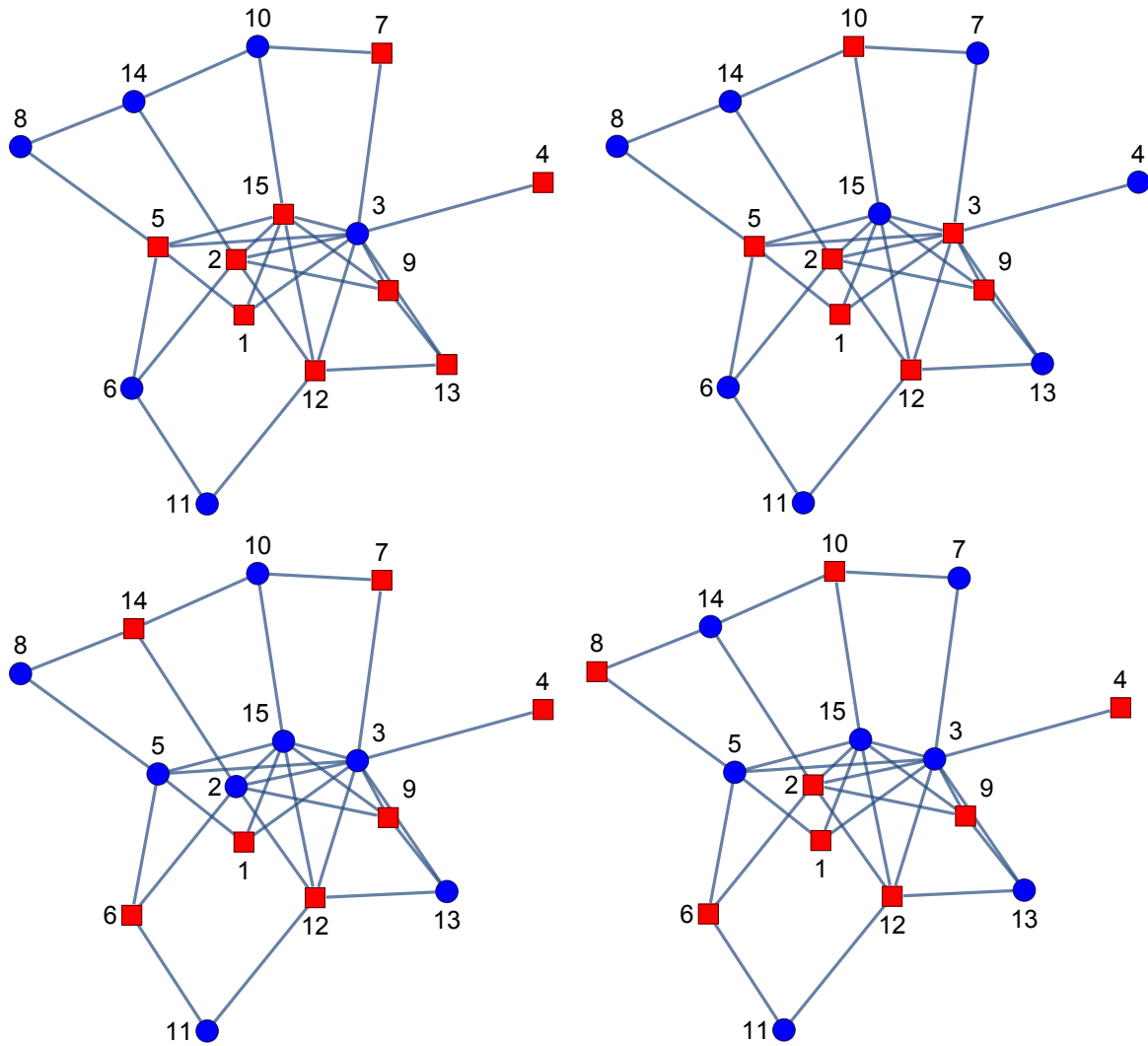


Figure 10. Graphical representation of a subset of the eigenvectors of the Laplacian of a uniform network with 15 nodes and 29 edges corresponding to the four largest natural frequencies (top left: $\Omega_1^2 - \Omega^2 \approx 10.12$, top right: $\Omega_2^2 - \Omega^2 \approx 8.37$, bottom left: $\Omega_3^2 - \Omega^2 \approx 7.39$, and bottom right: $\Omega_4^2 - \Omega^2 \approx 5.85$). Here, circles (blue) and squares (red) denote positive and negative elements of the corresponding eigenvector/mode shape.

with $v^T a \approx -0.08$. For both of these, $g_n \neq 0$ for all n . We consequently expect persistence of such a period-2 attractor over some range of values of the learning rate ρ . Indeed, for the first period-2 attractor, the two points along the orbit are characterized by the form

$$(34) \quad a = \left(0 \quad \frac{1-\rho}{2-\rho} \quad 1 \quad 0 \quad \frac{1}{2-\rho} \quad \frac{1}{2-\rho} \quad 1 \quad 0 \quad 0 \quad 0 \quad 0 \quad 0 \quad 1 \quad 0 \quad 1 \right)^T$$

and

$$(35) \quad a = \left(0 \quad \frac{1}{2-\rho} \quad 1 \quad 0 \quad \frac{1-\rho}{2-\rho} \quad \frac{1-\rho}{2-\rho} \quad 1 \quad 0 \quad 0 \quad 0 \quad 0 \quad 0 \quad 1 \quad 0 \quad 1 \right)^T,$$

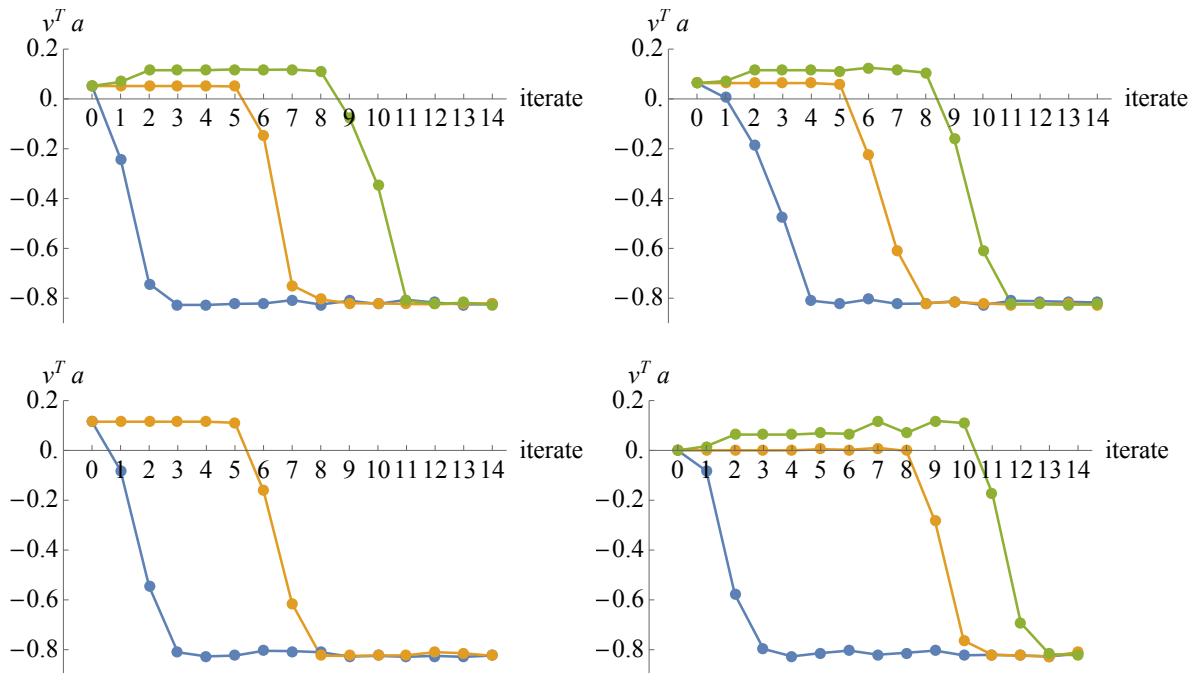


Figure 11. Iterated dynamics on the network in the top-left panel of Figure 10 with initial conditions near each of the four semistable fixed points described in the text and $\rho = 1$. Here, uniform additive noise on the interval $[-0.02, 0.02]$ is introduced after the fourth iterate, while ensuring that the components of the amplitude vector remain in $[0, 1]$. The existence of open insets is evidenced by metastable dynamics, with transient anchoring of $v^T a$ at predicted values, prior to convergence to the asymptotically stable fixed point.

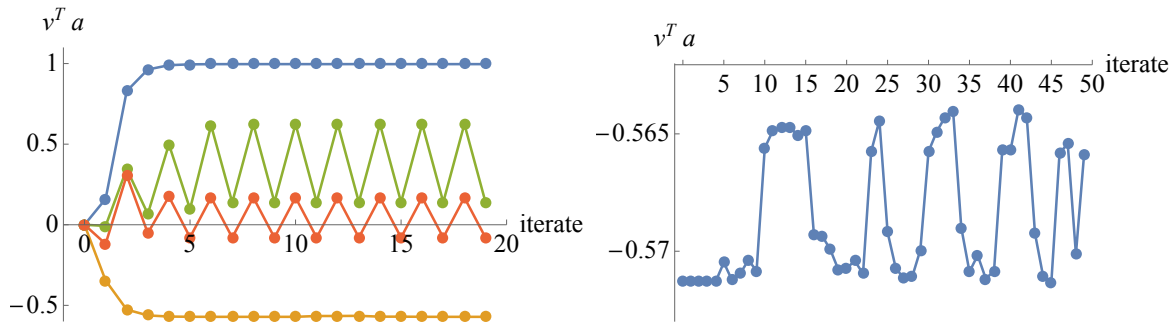


Figure 12. Example iterated dynamics on the network in the bottom-right panel of Figure 10 with initial conditions near the trivial fixed point $a^* = 0$ (left panel) and near a cycle of connecting transitions (right panel) for $\rho = 0.8$. In each case, uniform additive noise on the interval $[-0.001, 0.001]$ is introduced after the fourth iterate, while ensuring that the components of the amplitude vector remain in $[0, 1]$. The existence of two attractive period-2 orbits verifies the theoretical prediction in the text.

and similarly for the other period-2 attractor. By evaluating g_n across the network on each of these points, we predict a *border-collision bifurcation* [41] associated with a zero-crossing of g_n for some n when $\rho \approx 0.7718$ and $\rho \approx 0.8803$. The attractor is thus expected to persist on the interval between these values, an expectation that is borne out by numerical simulations.

4. Discussion.

4.1. System collapse. From the analysis in section 3, we conclude that the optimal selection of the subset of senders, for a given mode shape v and natural frequency Ω_m , is locally asymptotically stable under the proposed learning dynamics provided that the neighborhood of every node includes nodes in P_+ . Even when this is the case, we cannot exclude the possibility of an inset of the semistable fixed point at $a^* = 0$ with an open interior. Trajectories based at initial conditions within this inset experience convergence toward a state in which the network entirely fails to resonate with the exogenous excitation, in spite of its spectral structure. Such a failure to differentiate tasks across the network may be characterized as a *collapse* of the system, even though $a^* = 0$ is not a sink for all nearby trajectories. Indeed, small amounts of noise are enough to perturb an incoming trajectory, once sufficiently close to $a^* = 0$, so as to leave the inset and, potentially, converge toward an asymptotically stable fixed point. Although the dynamics remain near such an asymptotically stable fixed point even in the presence of small amounts of noise, sufficiently large perturbations may again place a trajectory in the inset of $a^* = 0$, leading to near-collapse. Since the inset is expected to contain an open interior, there is nothing special about such perturbations, and collapse may be predicted with some finite likelihood as a function of the distribution of the noise process.

While the inset of an unstable fixed point in a smooth dynamic system is expected to be of measure zero, this is not the case for the piecewise-defined dynamics of the learning algorithm. For example, the fixed point at $a^* = 0$ lives on the boundary of the system discontinuity, where $g_n = 0$ for one or several nodes. In such a case, attraction and departure may each be restricted to one side of the discontinuity, allowing for an inset of finite measure. In this system, collapse is not a function of a change to a system parameter, as in classical bifurcation analysis, but simply the result of sufficiently large perturbations in initial conditions. We conjecture that a similar phenomenology may explain failures of task differentiation in naturally occurring multi-agent systems, e.g., social insect societies [2, 35].

4.2. Network robustness. As shown in subsection 3.1, it is possible to grow an existing network in a systematic way, while ensuring sustained resonance at a given natural frequency and with a mode shape whose restriction to the original network is preserved. We may envision such growth as a defensive mechanism that builds redundancy into the network and shields its core from harm by increasing the relative cross-section of inconsequential nodes. For example, to the extent that we can attach neutral nodes to the original core (accompanied by required reductions to the grounding stiffnesses), these reduce the relative exposure of core nodes to targeted harm. They do so without affecting the optimal assignment of nodes as senders or receivers and without affecting the behavior of the proposed learning algorithm.

The attachment of a single new node (or a uniform network of new nodes)—with grounding stiffness equal to the square of a natural frequency—to a single node in the original core provides a mechanism for redundancy. A failure of the core node may be detected by the attached network and any of the new nodes may substitute for the original core node (provided that its grounding stiffness is appropriately adjusted). If the optimal selection of the subset of senders is asymptotically stable under the learning paradigm, then this remains the case also

when such redundancy is introduced to nodes in P_+ . Stability is lost, however, if redundancy is (also) added to nodes in P_- . Moreover, because of the orthogonality of the matrix V (even in the case of a nonuniform network), the addition of a sufficient number of redundant nodes may result in a reduction in the optimal value of $\|u_{ss}(t)\|$ relative to the value obtained for the original core. We may overcome the loss of stability simply by excluding the redundant nodes from the learning algorithm, requiring that their excitation sensitivity be identical to that of the associated core node. The possible reduction in the optimal value of $\|u_{ss}(t)\|$ may be avoided by placing limits on the number of nodes in each added network.

5. Conclusions. We studied task differentiation in the excitation sensitivity across the nodes of a network filter, a system of coupled linear oscillators. We showed that optimal assignments of excitation sensitivities correspond to the designation of subsets of nodes as senders, directly excited by the exogenous signals, with their complement constituting a collection of receivers whose steady-state behavior is only indirectly a function of the excitation. We analyzed the dynamics of an iterated learning paradigm that seeks to arrive at an optimal assignment of excitation sensitivities only through local information and documented nontrivial behavior in an intuitive, but nonsmooth formulation for the learning updates.

Outside of the periodic one-dimensional lattice with only nearest-neighbor coupling, the network filters considered here are not intended as models of an actual mechanical system, as interference between coupling springs makes a physical realization challenging at best. Instead, the objective is to consider a relevant phenomenology, viz., frequency filtering, coupled to a paradigm for emergent task differentiation as an example of how local interactions may be responsible both for the collective function of the system, as well as for the adaptation of the system to environmental constraints.

In the introduction, we indicated inspiration from the study of social insects, notably honey bee colonies, in which social interactions have been shown to contribute to the self-organization of tasks. We have no evidence to suggest that honey bee colonies act as linear frequency filters. Notably, their interactions constitute a time-dependent network, for which any notion of topology is restricted to some suitable time aggregate. (For network analysis of time-dependent trophallaxis interactions in honey bee colonies, see [14].) Moreover, task differentiation in such insect societies may be alternatively triggered by spatially localized needs, rather than by a collective global behavior.

In spite of the tenuous connection to naturally occurring networks, we believe that the network filter context affords an opportunity to understand effects of temporal sequencing (cf. [5]) and of the possible presence of endogenous signal sources within the system, as would be the case in an active filter. While the above analysis takes the network topology as given, it also informs the inverse question of topology optimization that seeks to identify a network structure for which the learning paradigm achieves robust and optimal task differentiation. We leave these questions for future study.

Acknowledgments. The authors thank Gene Robinson and Tim Gernat for providing inspiration for the present study by sharing their knowledge about the phenomenology behind division of labor in honey bee colonies and the possible influence of social interactions.

REFERENCES

- [1] R. ALBERT, H. JEONG, AND A.-L. BARABÁSI, *Error and attack tolerance of complex networks*, Nature, 406 (2000), pp. 378–382, <https://doi.org/10.1038/35019019>.
- [2] A. B. BARRON, *Death of the bee hive: Understanding the failure of an insect society*, Current Opinion Insect Sci., 10 (2015), pp. 45–50, <https://doi.org/10.1016/j.cois.2015.04.004>.
- [3] S. N. BESHES AND J. H. FEWELL, *Models of division of labor in social insects*, Ann. Rev. Entomology, 46 (2001), pp. 413–440, <https://doi.org/10.1146/annurev.ento.46.1.413>.
- [4] S. K. BUTLER, *Eigenvalues and Structures of Graphs*, Ph.D. thesis, University of California, San Diego, 2008.
- [5] D. CHARBONNEAU, B. BLONDER, AND A. DORNHAUS, *Social insects: A model system for network dynamics*, in Temporal Networks, P. Holme and J. Saramäki, eds., Springer, New York, 2013, pp. 217–244, <https://doi.org/10.1007/978-3-642-36461-7-11>.
- [6] D. CHARBONNEAU AND A. DORNHAUS, *When doing nothing is something. How task allocation strategies compromise between flexibility, efficiency, and inactive agents*, J. Bioecon., 17 (2015), pp. 217–242, <https://doi.org/10.1007/s10818-015-9205-4>.
- [7] D. COCKBURN AND Z. KOBTI, *Agent specialization in complex social swarms*, Stud. Comput. Intell., 248 (2009), pp. 77–89, https://doi.org/10.1007/978-3-642-04225-6_5.
- [8] T. COLETTA AND P. JACQUOD, *Linear stability and the Braess paradox in coupled-oscillator networks and electric power grids*, Phys. Rev. E, 93 (2016), 032222, <https://doi.org/10.1103/PhysRevE.93.032222>.
- [9] C. D. CORSO, A. DICKHERBER, W. D. HUNT, AND P. J. EDMONSON, *Passive sensor networks based on multi-element ladder filter structures*, in Proceedings of IEEE Sensors, 2008, pp. 538–541, <https://doi.org/10.1109/ICSENS.2008.4716496>.
- [10] P. CRUCITTI, V. LATORA, M. MARCHIORI, AND A. RAPISARDA, *Error and attack tolerance of complex networks*, Phys. A, 340 (2004), pp. 388–394, <https://doi.org/10.1016/j.physa.2004.04.031>.
- [11] T. H. F. DAUGHERTY, A. L. TOTH, AND G. E. ROBINSON, *Nutrition and division of labor: Effects on foraging and brain gene expression in the paper wasp polistes metricus*, Mol. Ecol., 20 (2011), pp. 5337–5347, <https://doi.org/10.1111/j.1365-294X.2011.05344.x>.
- [12] F. DÖRFLER, M. CHERTKOV, AND F. BULLO, *Synchronization in complex oscillator networks and smart grids*, Proc. Nat. Acad. Sci., 110 (2013), pp. 2005–2010, <https://doi.org/10.1073/pnas.1212134110>.
- [13] A. DUARTE, F. J. WEISSING, I. PEN, AND L. KELLER, *An evolutionary perspective on self-organized division of labor in social insects*, Ann. Rev. Ecol. Evol. Syst., 42 (2011), pp. 91–110, <https://doi.org/10.1146/annurev-ecolsys-102710-145017>.
- [14] T. GERNAT, V. D. RAO, M. MIDDENDORF, H. DANKOWICZ, N. GOLDENFELD, AND G. E. ROBINSON, *Bursty interaction patterns and rapid spreading dynamics in honey bee social networks*, in review, 2017.
- [15] D. M. GORDON, *From division of labor to the collective behavior of social insects*, Behav. Ecol. Sociobiol., 70 (2016), pp. 1101–1108, <https://doi.org/10.1007/s00265-015-2045-3>.
- [16] P. HAGEDORN AND S. TALIAFERRO, *Some remarks on dynamic receptance, stiffness, and impedance of mechanical systems*, Z. Angew. Math. Phys., 37 (1986), pp. 134–149, <https://doi.org/10.1007/BF00955524>.
- [17] J. D. HART, J. P. PADE, T. PEREIRA, T. E. MURPHY, AND R. ROY, *Adding connections can hinder network synchronization of time-delayed oscillators*, Phys. Rev. E, 92 (2015), 022804, <https://doi.org/10.1103/PhysRevE.92.022804>.
- [18] Z.-Y. HUANG AND G. E. ROBINSON, *Regulation of honey bee division of labor by colony age demography*, Behav. Ecol. Sociobiol., 39 (1996), pp. 147–158, <https://doi.org/10.1007/s002650050276>.
- [19] S. R. HUDDY AND J. SUN, *Master stability islands for amplitude death in networks of delay-coupled oscillators*, Phys. Rev. E, 93 (2016), 052209, <https://doi.org/10.1103/PhysRevE.93.052209>.
- [20] M. I. HUSSEIN, M. J. LEAMY, AND M. RUZZENE, *Dynamics of phononic materials and structures: Historical origins, recent progress, and future outlook*, Appl. Mech. Rev., 66 (2014), 040802, <https://doi.org/10.1115/1.4026911>.
- [21] Y. KANG AND G. THERAULAZ, *Dynamical models of task organization in social insect colonies*, Bull. Math. Biol., 78 (2016), pp. 879–915, <https://doi.org/10.1007/s11538-016-0165-1>.

- [22] I. LEONCINI, Y. LE CONTE, G. COSTAGLIOLA, E. PLETTNER, A. L. TOTH, M. WANG, Z. HUANG, J.-M. BÉCARD, D. CRAUSER, K. N. SLESSOR, AND G. E. ROBINSON, *Regulation of behavioral maturation by a primer pheromone produced by adult worker honey bees*, Proc. Nat. Acad. Sci., 101 (2004), pp. 17559–17564, <https://doi.org/10.1073/pnas.0407652101>.
- [23] Z. LEVNAJIĆ, *Emergent multistability and frustration in phase-repulsive networks of oscillators*, Phys. Rev. E, 84 (2011), 016231, <https://doi.org/10.1103/PhysRevE.84.016231>.
- [24] H. LIU, M. DOLGUSHEV, Y. QI, AND Z. ZHANG, *Laplacian spectra of a class of small-world networks and their applications*, Sci. Rep., 5 (2015), 9024, <https://doi.org/10.1038/srep09024>.
- [25] W. LIU, A. F. T. WINFIELD, J. SA, J. CHEN, AND L. DOU, *Towards energy optimization: Emergent task allocation in a swarm of foraging robots*, Adapt. Behav., 15 (2007), pp. 289–305, <https://doi.org/10.1177/1059712307082088>.
- [26] J. LUNZE, *Complete synchronisation of linear oscillator networks*, Internat. J. Control, 85 (2012), pp. 800–814, <https://doi.org/10.1080/00207179.2012.666805>.
- [27] F. MANFREDINI, C. LUCAS, M. NICOLAS, L. KELLER, D. SHOEMAKER, AND C. M. GROZINGER, *Molecular and social regulation of worker division of labour in fire ants*, Mol. Ecol., 23 (2014), pp. 660–672, <https://doi.org/10.1111/mec.12626>.
- [28] T. MATSUNO, Y. KIKKAWA, M. IGUCHI, K. TOKO, AND K. YAMAFUJI, *Periodic signal learning and recognition in coupled oscillators*, J. Phys. Soc. Japan, 63 (1994), pp. 1194–1204, <https://doi.org/10.1143/JPSJ.63.1194>.
- [29] D. MERKLE, M. MIDDENDORF, AND A. SCHEIDLER, *Task allocation in organic computing systems: Networks with reconfigurable helper units*, Int. J. Auton. Adapt. Comm. Syst., 8 (2015), pp. 60–80, <https://doi.org/10.1504/IJAACS.2015.067695>.
- [30] D. P. MERSCH, *The social mirror for division of labor: What network topology and dynamics can teach us about organization of work in insect societies*, Behav. Ecol. Sociobiol., 70 (2016), pp. 1087–1099, <https://doi.org/10.1007/s00265-016-2104-4>.
- [31] H. NAGARAJAN, S. RATHINAM, S. DARBHA, AND K. RAJAGOPAL, *Algorithms for synthesizing mechanical systems with maximal natural frequencies*, Nonlinear Anal. Real World Appl., 13 (2012), pp. 2154–2162, <https://doi.org/10.1016/j.nonrwa.2012.01.010>.
- [32] B. J. OLSON, S. W. SHAW, C. SHI, C. PIERRE, AND R. G. PARKER, *Circulant matrices and their application to vibration analysis*, Appl. Mech. Rev., 66 (2014), 040803, <https://doi.org/10.1115/1.4027722>.
- [33] J. P. PADE AND T. PEREIRA, *Improving network structure can lead to functional failures*, Sci. Rep., 5 (2015), 9968, <https://doi.org/10.1038/srep09968>.
- [34] R. E. PAGE, JR., AND S. D. MITCHELL, *Self-organization and the evolution of division of labor*, Apidologie, 29 (1998), pp. 171–190, <https://doi.org/10.1051/apido:19980110>.
- [35] C. J. PERRY, E. SØVIK, M. R. MYERSCOUGH, AND A. B. BARRON, *Rapid behavioral maturation accelerates failure of stressed honey bee colonies*, Proc. Nat. Acad. Sci., 112 (2015), pp. 3427–3432, <https://doi.org/10.1073/pnas.1422089112>.
- [36] G. E. ROBINSON, *Regulation of division of labor in insect societies*, Ann. Rev. Entomology, 37 (1992), pp. 637–665, <https://doi.org/10.1146/annurev.en.37.010192.003225>.
- [37] V. ROMERO-GARCÍA, J. V. SÁNCHEZ-PÉREZ, AND L. M. GARCIA-RAFFI, *Tunable wideband bandstop acoustic filter based on two-dimensional multiphysical phenomena periodic systems*, J. Appl. Phys., 110 (2011), 014904, <https://doi.org/10.1063/1.3599886>.
- [38] H. SAKAGUCHI, *Learning rules for an oscillator network*, Phys. Lett. A, 174 (1993), pp. 289–292, [https://doi.org/10.1016/0375-9601\(93\)90140-U](https://doi.org/10.1016/0375-9601(93)90140-U).
- [39] M. O. F. SARKER, T. S. DAHL, E. ARCAUTE, AND K. CHRISTENSEN, *Local interactions over global broadcasts for improved task allocation in self-organized multi-robot systems*, Robot. Auton. Syst., 62 (2014), pp. 1453–1462, <https://doi.org/10.1016/j.robot.2014.05.015>.
- [40] T. D. SEELEY, *Honeybee Democracy*, Princeton University Press, Princeton, NJ, 2010.
- [41] D. J. W. SIMPSON, *Border-collision bifurcations in \mathbb{R}^N* , SIAM Rev., 58 (2016), pp. 177–226, <https://doi.org/10.1137/15M1006982>.
- [42] Y. SUGITANI, K. KONISHI, AND N. HARA, *Delay- and topology-independent design for inducing amplitude death on networks with time-varying delay connections*, Phys. Rev. E, 92 (2015), 042928, <https://doi.org/10.1103/PhysRevE.92.042928>.

- [43] J. O. VASSEUR, P. A. DEYMIER, M. BEAUGEOIS, Y. PENNEC, B. DJAFARI-ROUHANI, AND D. PREVOST, *Experimental observation of resonant filtering in a two-dimensional phononic crystal waveguide*, *Z. Kristallographie*, 220 (2005), pp. 829–835, <https://doi.org/10.1524/zkri.2005.220.9-10.829>.
- [44] X. WANG AND P. VAN MIEGHEM, *Orthogonal eigenvector matrix of the Laplacian*, in Proceedings of the 11th International Conference on Signal-Image Technology and Internet-Based Systems, 2015, pp. 358–365, <https://doi.org/10.1109/SITIS.2015.35>.
- [45] Y. WANG, O. KAFTANOGLU, C. S. BRENT, R. E. PAGE, AND G. V. AMDAM, *Starvation stress during larval development facilitates an adaptive response in adult worker honey bees (*apis mellifera l.*)*, *J. Exp. Biol.*, 219 (2016), pp. 949–959, <https://doi.org/10.1242/jeb.130435>.
- [46] D. ZHANG, G. XIE, J. YU, AND L. WANG, *Adaptive task assignment for multiple mobile robots via swarm intelligence approach*, *Robot. Auton. Syst.*, 55 (2007), pp. 572–588, <https://doi.org/10.1016/j.robot.2007.01.008>.